

Spin-orbit torque-mediated spin-wave excitation as an alternative paradigm for femtomagnetism

G. P. Zhang* and M. Murakami

Department of Physics, Indiana State University, Terre Haute, IN 47809, USA

Y. H. Bai

Office of Information Technology, Indiana State University, Terre Haute, IN 47809, USA

Thomas F. George

*Office of the Chancellor and Departments of
Chemistry & Biochemistry and Physics & Astronomy,
University of Missouri-St. Louis, St. Louis, MO 63121, USA*

X. S. Wu

School of Physics, Nanjing University, Nanjing 210093, China

(Dated: December 5, 2019)

Abstract

Laser-induced femtosecond demagnetization, femtomagnetism, offers a potential route to develop faster magnetic storage devices. It is generally believed that the traditional spin-wave theory, which is developed for thermally driven slow demagnetization, can not explain this rapid demagnetization by design. Here we show that this traditional spin-wave theory, once augmented by laser-induced spin-orbit torque, provides a highly efficient paradigm for demagnetization, by capturing low-energy spin-wave excitation that is absent in existing mechanisms. Our paradigm is different from existing ones, but does not exclude them. Microscopically, we find that optical spin-orbit torque generates massive spin waves across several hundred lattice sites, collapsing the long-range spin-spin correlation within 20 fs. Our finding does not only explain new experiments, but also establishes an alternative paradigm for femtomagnetism. It is expected to have far-reaching impacts on future research.

I. INTRODUCTION

Magnetic storage technology is the backbone of information technology and relies on a fast manipulation of magnetic bits in hard drives. However, the traditional norm using a faster magnetic field to flip spins leads to a nondeterministic switching [1]. Twenty years ago, Beaurepaire and coworkers [2] discovered that a femtosecond laser pulse could demagnetize nickel thin films on a much faster time scale. Such a rapid demagnetization is generic and has been found in various magnetic systems [3–5]. But despite enormous efforts, its underlying mechanism is still under intense debate [6]. To this end, at least four mechanisms have been proposed (see Fig. 1). The role of spin-orbit coupling in demagnetization was recognized first in [7], and shows up in many systems [8–11]. One suggestion is that demagnetization proceeds by transferring the spin angular momentum to the orbital angular momentum through spin-orbit coupling [12, 13], or to the phonon subsystem [14–16] through Elliot-Yafet scattering with phonons or impurities [17, 18]. However, whether the spin transfers angular momentum to phonons is unclear since they only measured the X-ray diffraction signal [16]. Another suggestion is spin superdiffusion [19, 20]. Each of proposed mechanisms alone is insufficient to explain the experimental findings [21–26]. Spin-wave excitation (magnon) was also proposed several times before [12, 27–31]. It is possible to use spin transfer torque to drive spin dynamics [32]. Recently Eich and coworkers [33] reported the band mirroring effect, suggesting spin flipping, and Tengdin *et al.* [34] reported an ultrafast magnetic phase transition with 20 fs. More recently Chen and Wang [35] revealed that spin disorder is crucial to demagnetization. But further investigations in spin-wave excitation have been scarce [36]. The direct connection between demagnetization and spin-wave excitation is missing.

Here we aim to establish an alternative paradigm for laser-induced femtosecond demagnetization that is based on the spin-orbit torque and rapid spin-wave propagation. We employ a system of more than 1 million spins and adopt an atomic spin model that includes both the exchange interaction between spins and spin-orbit coupling, and takes into account the interaction between the laser pulse and our system realistically. We find that the laser-induced spin-orbit torque [32] starts a chain of action from spin flipping to demagnetization, triggers the spin precession, and generates a massive spin wave. The spin wavelength is over hundreds of lattice sites, so the energy cost is extremely low. A laser pulse of fluence 0.1 mJ/cm^2 can quench the spin angular momentum of $0.3\hbar$ by -20% . We observe the

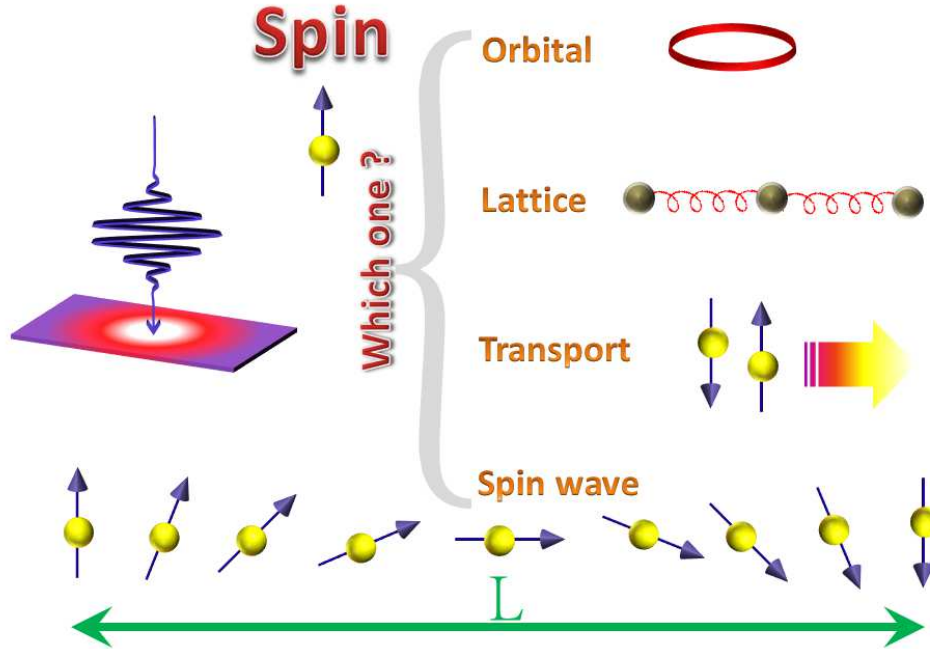


FIG. 1. Laser-induced ultrafast demagnetization has several possible mechanisms from spin-orbit coupling to spin waves. On the left, we show a schematic of a typical experiment, where a laser pulse impinges on a ferromagnetic thin film, with a finite radius and penetration depth. Bottom: Alternative paradigm of femtomagnetism based on the spin-wave picture, where a spin wave may cover many lattice sites.

long-range spin-spin correlation collapsing within 20 fs, consistent with the experimental observation [34]. Band mirroring [33] is a natural consequence of spin-wave excitation. Our finding establishes an alternative paradigm for laser-induced ultrafast demagnetization and should have a profound impact in the future.

The paper is arranged as follows. In Sec. II, we develop our concept of demagnetization through spin-wave excitation. In Sec. III, we present our theoretical formalism which includes the model construction and numerical algorithm. Section III is devoted to the results. We first investigate how the laser helicity, exchange interaction, spin-orbit coupling and laser field amplitude affect the demagnetization, and then demonstrate the collapse of the spin-spin correlation function. We resolve the spin change in time and space, and present the images of all the spins in real space. A movie is provided. The discussion and alternative paradigm are presented in Sec. IV. We conclude this paper in Sec. V.

II. SPIN-WAVE EXCITATION UNDER LASER EXCITATION: CONCEPTS

Modern magnetism theory has two competing pictures of magnetic excitation. In the itinerant Stoner model, spins are mobile and follow the charge, so a band structure description is favored, where the spin majority and minority bands shift toward each other, and consequently the spin moment is reduced. In the localized Heisenberg picture, the spin degree of freedom is decoupled from the charge. The module of spin at each lattice site is constant, but the spin orientation is not.

Consider a one-dimensional spin chain in the Heisenberg picture. For a traveling wave and under the linear response approximation, the transverse components at each site are $s_x^j = u \cos(jka - \omega t)$, and $s_y^j = u \sin(jka - \omega t)$, where j is the site index, u is the amplitude of spin wave, k is the spin-wave vector, a is the lattice constant, ω is the spin-wave angular frequency, and t is time. The longitudinal component is $s_z^j = s$. At each site j , the spin module is $\sqrt{s^2 + u^2}$, which is independent of the site index. The total spin \mathbf{S} of the system along the x , y and z axes is $(\sum_j s_x^j, \sum_j s_y^j, \sum_j s_z^j)$. If the summation is over one wavelength of the spin wave, then $\mathbf{S} = (0, 0, Ns)$, where the transverse components all cancel out and N is the total number of lattice sites.

The Heisenberg picture provides a simple explanation of demagnetization. Consider a simple model with two spins, \mathbf{s}_1 and \mathbf{s}_2 , with modules $|\mathbf{s}_1|$ and $|\mathbf{s}_2|$. The total spin is $\mathbf{S} = \mathbf{s}_1 + \mathbf{s}_2$. To determine the module S of \mathbf{S} , we compute $\mathbf{S} \cdot \mathbf{S}$ as follows:

$$S^2 = \mathbf{S} \cdot \mathbf{S} = |\mathbf{s}_1|^2 + |\mathbf{s}_2|^2 + 2\mathbf{s}_1 \cdot \mathbf{s}_2 . \quad (1)$$

The last term in Eq. (1) depends on the spatial orientation of spins. As far as \mathbf{s}_1 and \mathbf{s}_2 misalign with respect to each other, the total spin is guaranteed to reduce. The total spin can be reduced to zero if these two spins are antiparallel to each other with the same module. For many spins, the traditional Heisenberg Hamiltonian is $H_0 = -J \sum_{ij} \mathbf{s}_i \cdot \mathbf{s}_j$, with J being the exchange coupling. The spin reorientation is described by the magnon excitation and the number of magnons is simulated by a Bose-Einstein distribution. Since the magnetization is proportional to $(S - \langle n \rangle)$, where $\langle n \rangle$ is the magnon number and S is the total spin in the ground state, as $\langle n \rangle$ increases, the magnetization decreases. How the spin reorients does not enter into the theory.

However, under laser excitation we have to explicitly describe how the spin reorients itself, and in the literature there is no agreement on how this occurs. In this study, we propose the

spin-orbit coupling (SOC) as the key driver for spin reorientation because its energy scale is comparable to the experimental time scale of several hundred femtoseconds. It is easy to understand how the spin is reorientated under SOC. Suppose that an electron 1 has spin \mathbf{s}_1 with its neighboring \mathbf{s}_2 . The laser field changes the orbital angular momentum \mathbf{l}_1 due to the dipole selection rule $\Delta l = \pm 1$. Then \mathbf{s}_1 is subject to an effective field, $\mathbf{B}_{\text{eff}} = -J\mathbf{s}_2 + \lambda\mathbf{l}_1$. \mathbf{s}_1 precesses and finally settles along \mathbf{B}_{eff} . The angle α between $-J\mathbf{s}_2$ and \mathbf{B} is determined by

$$\cos(\alpha) = \mathbf{B}_{\text{eff}} \cdot (-J\mathbf{s}_2) / (|\mathbf{B}_{\text{eff}}| |-J\mathbf{s}_2|) = \frac{s_2^2 - \frac{\lambda}{J}\mathbf{l}_1 \cdot \mathbf{s}_2}{\sqrt{(s_2^2 + \frac{\lambda^2}{J^2}l_1^2 - 2\frac{\lambda}{J}\mathbf{l}_1 \cdot \mathbf{s}_2)s_2^2}}. \quad (2)$$

The spin-orbit coupling is indispensable to spin reorientation. For instance, if $\lambda = 0$, then $\alpha = 0^\circ$, so the spin does not reorient. A nonzero α allows the spin to choose an angle that may be different from neighboring sites. This introduces a highly noncollinear spin configuration that can efficiently demagnetize a sample.

III. THEORETICAL FORMALISM

As can be seen below, in general α is very small. This presents a major challenge for numerical calculations. For instance, for $\alpha = 1^\circ$, to construct a spin wave of just one period, one must include at least 180 lattice sites along one direction to accommodate such a long spin wave (Fig. 1). We wonder whether our prior model that was developed for all-optical spin switching [37–41] could help. This model is very much similar to the traditional $t - J$ model, where the spin degree of freedom is taken into account by the Heisenberg exchange interaction, and the charge degree of freedom is taken into account by the hopping term between neighboring atoms. In our model, we add a twist by replacing the tight-binding term by a real-space kinetic energy and potential energy term, so we can easily include one extra term, spin-orbit interaction. With these conditions in mind, we have the Hamiltonian as [37–41],

$$H = \sum_i \left[\frac{\mathbf{p}_i^2}{2m} + V(\mathbf{r}_i) + \lambda \mathbf{l}_i \cdot \mathbf{s}_i - e\mathbf{E}(\mathbf{r}, t) \cdot \mathbf{r}_i \right] - \sum_{ij} J\mathbf{s}_i \cdot \mathbf{s}_j, \quad (3)$$

where the first term is the kinetic energy operator of the electron, the second term is the potential energy operator, λ is the spin-orbit coupling, and \mathbf{l}_i and \mathbf{s}_i are the orbital and spin angular momenta at site i in the unit of \hbar , respectively. The potential energy term $V(\mathbf{r}_i)$ takes the harmonic potential. We also tried other forms of potentials, but we find the

harmonic potential is the best to model our system. $\mathbf{E}(\mathbf{r}, t)$ is the electric field of the laser pulse and has a Gaussian shape in time and space, as described by

$$\mathbf{E}(\mathbf{r}, t) = \mathbf{A}(t) \exp\left[-\frac{(x - x_c)^2 + (y - y_c)^2}{R^2} - \frac{z}{d}\right], \quad (4)$$

where x and y are the coordinates in the unit of the site number, and d is the penetration depth of light. R is the radius of the laser spot. The field $\mathbf{A}(t)$ has a Gaussian shape in the time domain, with the amplitude A_0 . We employ left and right circularly (σ^+ , σ^-) or linearly polarized light (π), with the polarization plane in the sample plane (see Fig. 1). We do not include the relaxation processes since they only play an important role on a much longer time scale. Our model is designed to complement the first-principles theory, where a calculation with a large number of highly noncollinear spins is not possible. The strength of our model is that we can treat a system with lots of spins along different directions. We will come back to this below. Finally, we emphasize that our model includes the electronic excitation from the beginning because of four bracketed terms in Eq. (3). The essence of our model is that the charge dynamics of the electrons is described by the harmonic potential, while the spin dynamics of the electrons is described by the Heisenberg model.

We numerically solve the Heisenberg equation of motion [39] for the spin and other observables at site i as follows:

$$i\hbar \frac{d\mathbf{s}_i}{dt} = [\mathbf{s}_i, H]. \quad (5)$$

If the number of lattice sites is M , there are $9M$ differential equations, with $3M$ each for spin, position and velocity. The time spent also depends on the laser field amplitude and pulse duration. A typical run needs more than 48 hours on a single processor computer with 2.1 GHz, Intel Xeon(R). We normally output the system-averaged spin at each time step, but because of the huge volume of data, we only save all the spins at a few selected time steps.

IV. RESULTS

Our simulation box contains $N_x = N_y = 501$ sites along the x and y axes, with four monolayers ($N_z = 4$) along the z axis, with the total number of spins over a million. Our system lateral dimension is now comparable to the experimental domain size of 140 nm [23, 42, 43]. One big strength of our model is that our system size is much larger than any

TABLE I. Parameters used in our simulation.

| | |
|--|---------------------------|
| System size ($N_x \times N_y \times N_z$) | $501 \times 501 \times 4$ |
| Initial velocity \mathbf{V} ($\text{\AA}/\text{fs}$) | (0.0, 0.0, 1.0) |
| Initial spin \mathbf{s}_i (\hbar) | (0, 0, -0.3) |
| Exchange interaction J (eV/\hbar^2) | 0.1-1.0 |
| Spin-orbit coupling λ (eV/\hbar^2) | 0.01-0.06 |
| Laser duration T (fs) | 100 |
| Laser amplitude A_0 ($\text{V}/\text{\AA}$) | 0.002-0.05 |
| Photon energy $\hbar\omega$ (eV) | 1.6 |
| Helicity | σ^+, σ^-, π |
| Beam radius R | 100-200 |
| Beam center (x_c, y_c) | (250,250) |

prior theoretical simulation. Due to our current computer limitation, further increase of system size is not possible. Our laser duration is 100 fs, the photon energy is 1.6 eV, and the radius of the laser spot is $R = 100$ lattice sites, one-fifth of the simulation box. The laser field amplitude is $0.008 \text{ V}/\text{\AA}$, which can be converted to the laser fluence through [44], $F = \sqrt{2\pi n c \epsilon_0} A_0^2 \tau$, where n is the index of refraction, c is the speed of light, the permittivity in vacuum is $\epsilon_0 = 8.85 \times 10^{-12} \text{ C}^2/\text{Nm}^2$, and τ is the laser pulse duration. At $\hbar\omega = 1.6 \text{ eV}$, $n = 2.45$. For a pulse of 100 fs with $A_0 = 0.008 \text{ V}/\text{\AA}$, $F = 0.10435 \text{ mJ}/\text{cm}^2$, which is at the lower end of the experimental laser field amplitudes [44]. We take the bulk Ni's spin angular momentum ($s_z = 0.3\hbar$) as an example. We choose $J = 0.1 \text{ eV}/\hbar^2$ and $\lambda = 0.06 \text{ eV}/\hbar^2$ for Ni [7]. Other parameters are also considered. We list all the parameters used in this paper in Table I.

A. Dependence of demagnetization on system and laser parameters

Once we initialize the spin along the $-z$ axis, σ^+ and σ^- are no longer equivalent because the spin determines the quantization axis. Figure 2(a) shows a phase diagram of the transverse spin components $S_x = \sum_j s_x^j$ and $S_y = \sum_j s_y^j$ for σ^+ , σ^- and π light. The word ‘‘start’’ denotes the starting S_x and S_y . With arrival of the laser pulse, the laser helicity has a clear

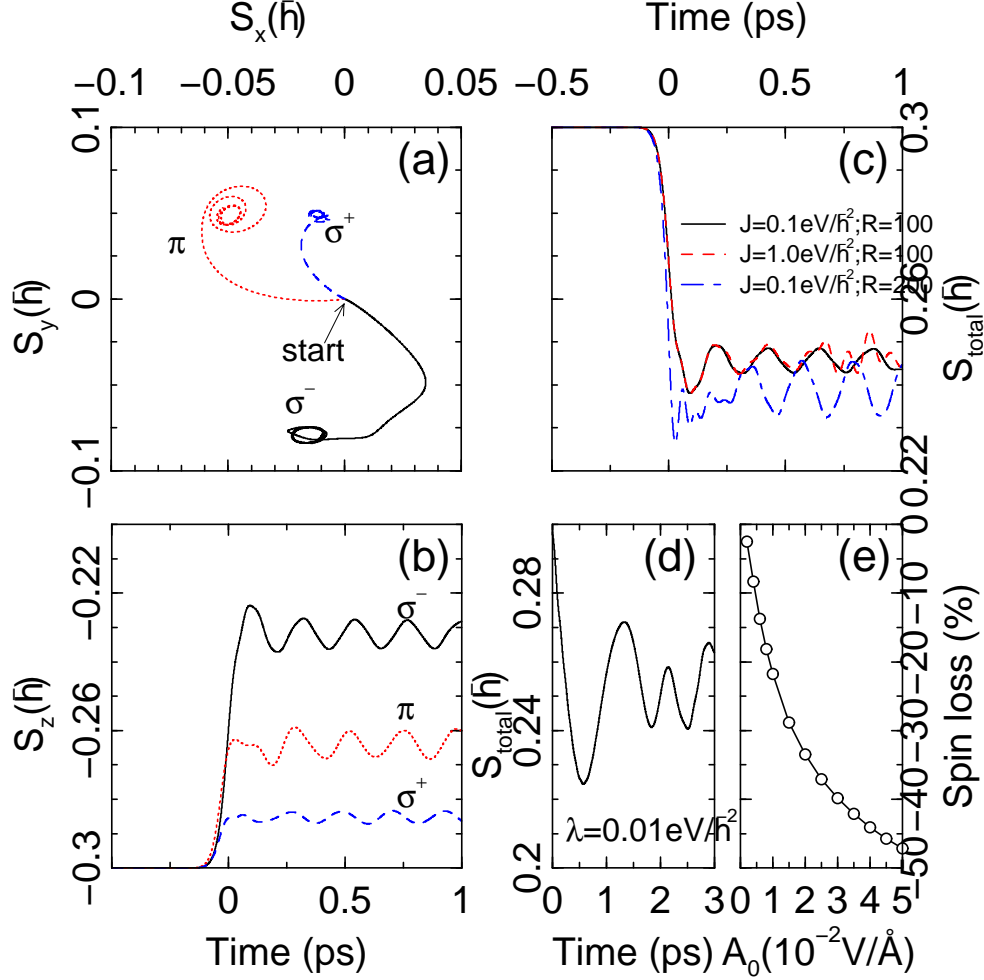


FIG. 2. (a) Phase diagram of the transverse components of the total spin for σ^+ , σ^- and π light. The initial point is denoted by “start”. (b) z component of the spin for σ^+ , σ^- and π light. σ^- has the strongest influence because of the spin configuration. (c) Dependence of the total spin as a function of time for two exchange interactions J and two beam radii R . Here a linearly polarized pulse (π) is employed. (d) Spin reduction with a reduced spin-orbit coupling. (e) Percentage loss of the spin as a function of laser field amplitude A_0 .

imprint on the phase diagram. For σ^- , the spin precesses toward the $+x$ and $-y$ axes before it settles down at $(-0.016, -0.078)\hbar$, with some oscillations. Under π excitation, the spin swings toward a large $-x$ value and then settles down at $(-0.047, -0.048)\hbar$, where S_x and S_y have a similar amplitude. σ^+ has the smallest effect because it only switches spins from up to down [45]. Once the spin points down, its effect is small. If we compare σ^+ and σ^- , we find their final spins lie opposite to each other. This strong helicity dependence is consistent

with our prior model study [45]. It is possible that our model does not include the itinerancy of the electrons sufficiently, so the helicity dependence is stronger from our model. A weak helicity dependence is obtained using the first-principles method [45]. Figure 2(b) shows the z component of the spin as a function of time. Regardless of helicity, S_z reduces sharply around 0 ps, and shifts to a new equilibrium. For each helicity, S_z changes differently, with the strongest change from σ^- (less negative). The period of the spin oscillation is same.

The helicity is not the only one that affects the spin. If we increase the radius of the laser spot to $R = 200$, we find the demagnetization increases (compare the solid and dot-dashed lines in Fig. 2(c)). To be more objective, Fig. 2(c) shows the total spin ($|\mathbf{S}|$). We find that the increase is much larger for σ^+ and π . The influence of the exchange interaction J on demagnetization is particularly interesting, but its role has been unclear. We choose two J 's, 0.1 and 1.0 eV/ \hbar^2 , and plot the results in Fig. 2(c). One sees that the demagnetization does not strongly depend on the exchange interaction. Its effect appears only at the later stage. The reason is simple. For our initial ferromagnetic spin configuration, the spin torque due to the exchange interaction is zero and can not flip spins. The exchange interaction has to wait until the spin flipping occurs. Since the spin-orbit torque is the only spin flipping term in our model, the influence of the exchange interaction is delayed. This points out an often neglected fact that even though the exchange interaction is stronger than the spin-orbit coupling, when the exchange interaction starts to play a role is not determined by the time scale of the exchange interaction alone. Although spin-orbit coupling λ is small, it dominates the initial spin dynamics. We can test this idea by reducing λ six times to $\lambda = 0.01$ eV/ \hbar^2 . Figure 2(d) shows the same total spin as a function of time. We notice that the first spin minimum appears at 577.7 fs, compared to 90.4 fs at $\lambda = 0.06$ eV/ \hbar^2 . This is a sixfold increase. Therefore, there is a direct one-to-one correspondence between the demagnetization time and the spin-orbit coupling. However, the amount of the spin reduction remains similar. To reduce the spin further, we can increase the laser field amplitude. Figure 2(e) shows a monotonic decrease of spin up to -50% with a field amplitude up to 0.05 V/ \AA . This amount of demagnetization agrees with the experimental observation [44, 46].

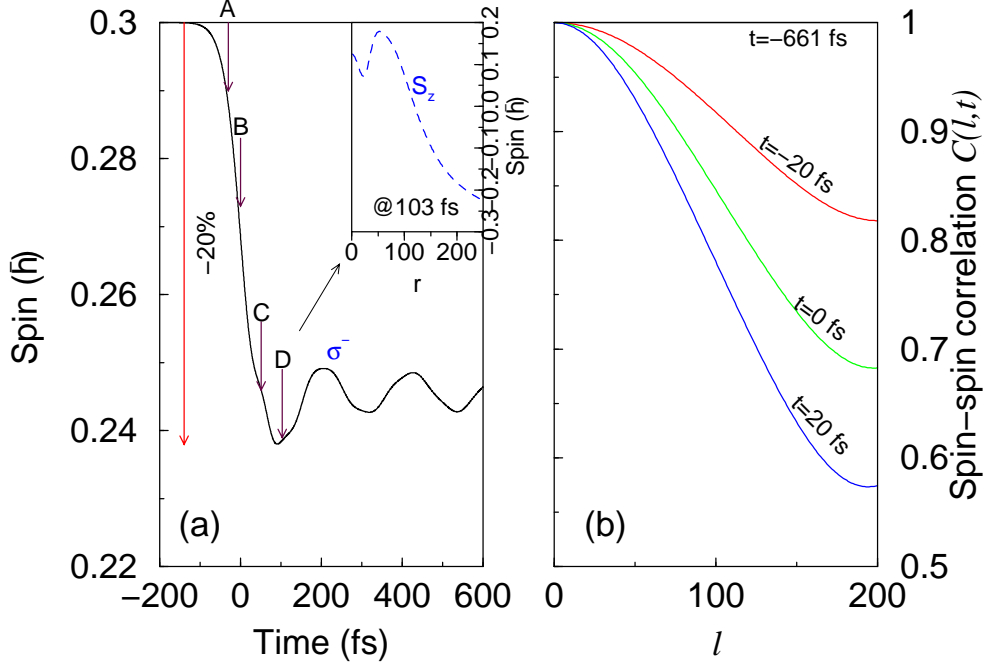


FIG. 3. (a) Strong demagnetization under a weak laser pulse of fluence 0.1 mJ/cm^2 and duration 100 fs. The spin reduction reaches -20% . To be objective, only the magnitude of spin is shown. Four arrows “A” to “D” denote four times, whose spins are spatially resolved in Fig. 4. The top inset shows the spatially integrated spin at “D” (103 fs) as a function of radius r . The spins are highly noncollinear, and close to the excitation center, the spin tilts toward the $+z$ axis. (b) The spin-spin correlation function $C(l, t)$ at five different times t , collapsing within 20 fs, as consistent with the experimental findings [34]. The correlation carries different information from demagnetization. l is the distance between two spins. In the ferromagnetic phase, the materials have a long-range order.

B. Spin-spin correlation collapse within 20 fs

So far, only the phenomenological spin diffusion model [19] can reproduce a comparable experimental spin reduction. Nearly all the first-principles calculations report a very small spin moment change [47, 48]. The above huge spin reduction, without a phenomenological treatment of laser excitation, is encouraging. This motivates us to thoroughly investigate what leads to strong demagnetization. We use $A_0 = 0.008 \text{ V/\AA}$ as an example. Figure 3(a) represents our key result that a weak laser pulse induces -20% spin reduction within 200 fs. The spin oscillation is very similar to the oscillation in the odd second harmonic

signal in Gd measured by Melnikov *et al.* [28], but they attributed it to the surface phonon vibration. Nevertheless, the fact that our frequency of 4.4 THz is comparable to theirs of 2.9 THz shows that their magnon wave packets are indeed coupled to the phonons. If we examine our results closer, we find that the spin percentage loss is not uniform across the slab. The inset of Fig. 3(a) shows an example at 103 fs (D in Fig. 3(a)) of spatially integrated spins with respect to the center of excitation, $S_z(r) = \sum_{i=1}^r s_z^i$, where r is the radius of the measurement. We notice that the spins (S_z) close to the excitation center reverse their directions to the $+z$ axis. Around $r = 100$, S_z is close to zero; and away from the center S_z remains unchanged since there is no strong excitation.

The above spatial information is useful to understand the phase transition. We compute the spin-spin correlation function $C(l, t)$ [36],

$$C(l, t) = \sum_{i:x,y} \frac{\mathbf{s}_i(t) \cdot \mathbf{s}_{i\pm l}(t)}{N_{x,y} |\mathbf{s}|^2}, \quad (6)$$

where the summation is over both the x and y axes, l measures the range of spin correlation across lattice sites, and $N_{x,y}$ is the normalization constant. It is expected that the ferromagnetic thin film has a long-range ordering in the beginning. We note in passing that this correlation function carries different information from demagnetization. Figure 3(b) illustrates that the correlation function is 1.0 long before laser excitation and around -20 fs reduces to 0.81. At $t = 20$ fs, the correlation function drops precipitously to 0.57 at $l = 200$. Collapsing of the spin-spin correlation is generic, regardless of laser helicity. When we use a π pulse, the correlation function $C(l, t)$ similarly collapses within 20 fs. This nicely explains why experimentally Tengdin *et al.* [34] reported a magnetic phase transition within 20 fs.

C. Space- and time-resolved demagnetization

To reveal further insight into demagnetization, it becomes necessary to resolve the spin change in real space. We choose four times, labeled by “A” through “D” in Fig. 3(a). Figure 4 (“Multimedia view”) shows a three-dimensional spin image snapshot for the entire first layer at these four times of (a) -31 fs, (b) 0 fs, (c) 51 fs and (d) 103 fs. The Multimedia view has a movie of a full-time-dependent spin evolution. To reduce the huge volume of data to a manageable level, in the figure we only retain one out of every 10 spins and zoom in the central portion of spins from lattice site 100 to 400 along the x and y axes. Spins

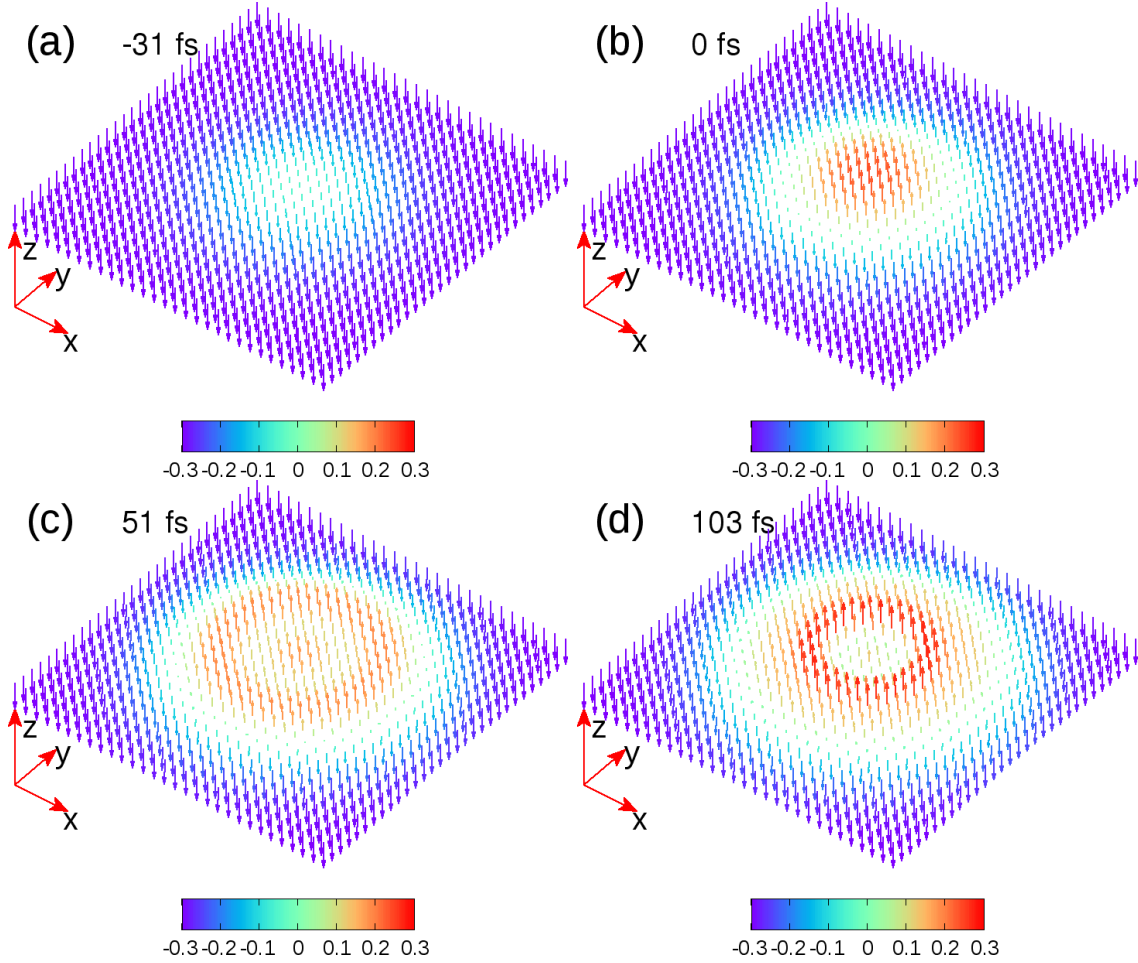


FIG. 4. Snapshot of spins at (a) -31 fs, (b) 0 fs, (c) 51 fs and (d) 103 fs. (a) and (b) show that the demagnetization starts with spin flipping at the center. In (c), spins are highly noncollinear and form the spin domains spreading outwards. A spin domain wall is built around the center. Spins close to the excitation center are reversed. In (d), two layers of spin waves appear. The color bar goes from the violet ($-0.3\hbar$) to the red ($0.3\hbar$). We only show one out of every ten spins within a region of 300×300 to reduce the huge volume of data. “Multimedia View”.

in the vicinity of our simulation box are not affected and not shown. Figure 4(a) shows that at -31 fs, the spins tilt away from the initial $-z$ axis to the xy plane, and the main change is at the center of the laser pulse, where the field amplitude is the strongest. Around 0 fs when the laser pulse peaks, spins in a small central region of 50 lattice sites reverse to the $+z$ axis (see 4(b)), and they collectively develop into a spin wave. But different from the traditional magnon excitation where the spin tilting is small, here the spins are highly noncollinear and can be completely flipped, so the majority (minority) spin becomes the

TABLE II. Spin propagation speed v_p . The speed of [50] changes from 0.017 nm/fs to 0.033 nm/fs and then back to 0.0148 nm/fs. The table lists the fastest speed. Experiments were carried out under different conditions for different samples. The x-ray scattering data consistently show a slower speed than that from the holography data. Additional near-field measurement is necessary. XMCD: x-ray magnetic circular dichroism.

| Sample | v_p (nm/fs) | Method | Reference |
|-----------------|---------------|-----------------|-----------|
| CoPt multilayer | 0.012-0.020 | XMCD+scattering | [51] |
| FePt (grain) | 0.033 | XMCD+scattering | [50] |
| CoPd | 0.2 | XMCD+Holography | [52] |
| Theory | 0.3-0.4 | | This work |

minority spin (majority), leading to the band mirroring effect observed experimentally [33]. The spin wave has a wavelength of 120 sites, or over 40 nm for fcc Ni, which is much bigger than the unit cell used in prior studies [48, 49].

Figure 4(c) shows that at 51 fs, the spin wave propagates outward, and its characteristic time is determined by the exchange interaction J . For our $J = 0.1 \text{ eV}/\hbar^2$, this approximately corresponds to 40 fs. The spread of the spin wave is consistent with those reported experimentally by von Korff Schmising *et al.* [52], but they attributed it to spin-polarized electron transport. We estimate the speed of spin-wave propagation at 1.2 lattice site per fs. Using the fcc Ni or bcc Fe lattice constant, we have a speed of 0.3 to 0.4 nm/fs, which is surprisingly close to the experimental value of 0.2 nm/fs [52], given many differences between experiment and theory. Therefore, we believe that their results are more consistent with the spin-wave propagation than with transport. If we accept the spin-wave picture, we now can understand why the demagnetization and spin-wave propagation appear in tandem. In the spin-wave picture, the spin wave is a precursor of demagnetization. In agreement with the experiment by Pfau *et al.* [51], our nanoscale spin walls are established during the demagnetization, which further explains why their spin correlation length can expand by 2.8 nm within 0.5 ps, since the spin wall is a consequence of spin waves and is not a regular magnetic domain wall which is much slower to establish. Spin propagation speed v_p is material dependent. The expansion of the width $d\xi$ can be computed from the momentum transfer dq , $d\xi = -(2\pi/q^2)dq$. From Pfau's experiment [51], $dq = 0.04q_{\text{peak}}$, where $q_{\text{peak}} = 42\mu\text{m}$, so

we get $d\xi = 5.98$ nm. Their time has a large uncertainty of 200 fs. Their v_p is estimated between 0.012 and 0.020 nm/fs. A faster speed than that in CoPt was found in FePt grains [50]. Table II summarizes the experimental results currently available, in comparison with our theory. Figure 4(d) shows that at 103 fs, the perimeter of the spin wall is defined, and spin waves can recoil from the wall. A hole is developed in the center. The further spread of the spin wave ceases from now on. We monitor the entire spin precession up to 900 fs and find no change.

V. DISCUSSION: AN ALTERNATIVE PARADIGM

Thermal demagnetization proceeds through a collective low-energy spin excitation driven by a thermal field. Laser-induced demagnetization is more complex. If the demagnetization proceeds through angular momentum transfer from the spin subsystem to the orbital subsystem, one should expect a surge of the orbital angular momentum during demagnetization, though it is not necessary. We can directly check this in our model. Figure 5(a) shows the system-averaged orbital angular momentum is extremely small, on the order of $0.01 \hbar$ for all three components, L_x , L_y and L_z , in agreement with the experiment [53]. This caps the maximum spin reduction through angular momentum transfer by no more than 3%.

How does such a small orbital momentum induce strong demagnetization? The inset in Fig. 5(a) illustrates that each spin is subject to at least two competing interactions: spin-orbit coupling and exchange interaction between neighboring spins. The spin tilting angle α between a spin \mathbf{s}_1 and its neighboring spin \mathbf{s}_2 is determined by Eq. (2). Since J , λ and \mathbf{s} are fixed, the only free parameter is the angle θ_{12} between \mathbf{l}_1 and \mathbf{s}_2 . The laser field enters through \mathbf{l}_i . It is important to realize that the direction of \mathbf{l}_i is controlled by the laser pulse, not by spin, so θ_{12} can take any value between 0° and 180° . We plot α as a function of θ_{12} . Figure 5(b) shows α has a maximum of about 1 degree at $\theta_{12} = 90^\circ$. This means that even assuming α remains constant, one needs 180 lattice sites to get a spin configuration completely reversed at the last lattice site with respect to the first site. This number matches our domain width of 240 sites. For each tilting, there is an energy cost due to the exchange interaction $-J\mathbf{s}_1 \cdot \mathbf{s}_2$. The exchange energy cost for $\alpha = 1^\circ$ can be estimated by subtracting the ground state energy from the energy of the spin tilt configuration, $J|\mathbf{s}|^2[1 - \cos(1^\circ)] = 1.371\mu\text{eV}$, if we choose $l = 0.01\hbar$, $J = 0.1$ eV/ \hbar^2 and

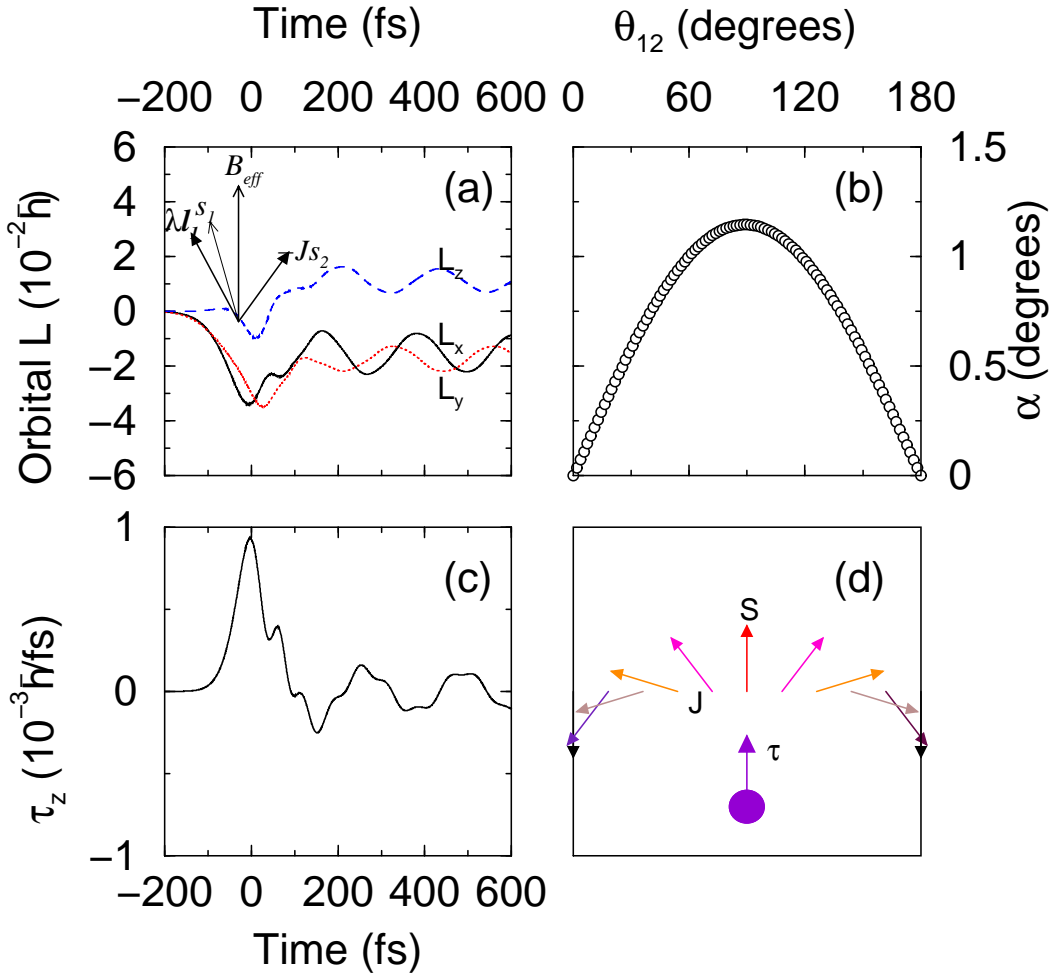


FIG. 5. (a) Time-evolution of system-averaged orbital angular momenta, L_x (solid line), L_y (dotted line) and L_z (dashed). The overall change is small, within $0.01\hbar$. Inset: Competition between the spin-orbit coupling and the exchange interaction. (b) Spin tilting angle α as a function of angle between the orbital angular momentum \mathbf{l}_1 at site 1 and spin \mathbf{s}_2 at site 2. A maximum is found at 90° . (c) Time-dependent spin-orbit torque. A large positive τ_z around 0 fs flips the spins. (d) Schematic of our alternative paradigm. The laser induces a strong spin-orbit torque τ on spin S . Through the exchange interaction J , the spin wave propagates. The spatial misalignment leads to a huge spin reduction.

$s = 0.3\hbar$. For the entire 240 sites, the energy cost is 0.33 meV. Such a low-energy spin-wave excitation is the origin of the strong demagnetization. We also understand why spin flips. Figure 5(c) shows that spin-orbit torque [39] $\tau_z = \lambda(\mathbf{L} \times \mathbf{S})_z$ around 0 fs is positive and large, so the spin flips from the $-z$ axis to the $+z$ axis. Figure 5(d) illustrates the key idea of our alternative paradigm: It is this spin-orbit torque that flips the spin, generates a highly

noncollinear spin wave and cancels the spins at different lattice sites.

VI. CONCLUSION

We have established an alternative paradigm for laser-induced ultrafast demagnetization. This alternative paradigm is based on the spin-orbit torque-induced spin-wave excitation. We employ a magnetic film with over one million spins, exchange-couple them, and take into account both spin-orbit coupling and realistic interaction with the laser field. By temporally and spatially resolving all the spins, we find that spin flipping starts at the center of excitation and generates a massive spin-wave extending across several hundred lattice sites. Small spin tilting from one site to next keeps the energy cost extremely low, leading to a highly efficient demagnetization. A pulse of 0.1 mJ/cm^2 is capable of reducing the spin of $0.3\hbar$ by 20%. Our alternative paradigm differs from prior proposed mechanisms in two aspects. First, our model captures low-energy spin-wave excitation. Second, we are able to describe these spin waves of wavelength over hundred lattices. Our finding does not only explain the band mirroring effect [33] and ultrafast magnetic phase transition within 20 fs [34], but opens the door to a fresh paradigm for laser-induced ultrafast demagnetization.

ACKNOWLEDGMENTS

We would like to thank Drs. Z. H. Chen and L. W. Wang (U. S. Lawrence Berkeley National Laboratory) for sending us their preprint that motivated the current study. We thank Tyler Jenkins for the assistance with Table II. GPZ, MM and YHB were supported by the U.S. Department of Energy under Contract No. DE-FG02-06ER46304 (GPZ, MM and YHB). Part of the work was done on Indiana State University's high performance Quantum and Obsidian clusters. The research used resources of the National Energy Research Scientific Computing Center, which is supported by the Office of Science of the U.S. Department of Energy under Contract No. DE-AC02-05CH11231. XSW acknowledges the support from NNSFC (No. 118742007) and the National Key R&D Program of China through Grant No. 2017YFA0303202.

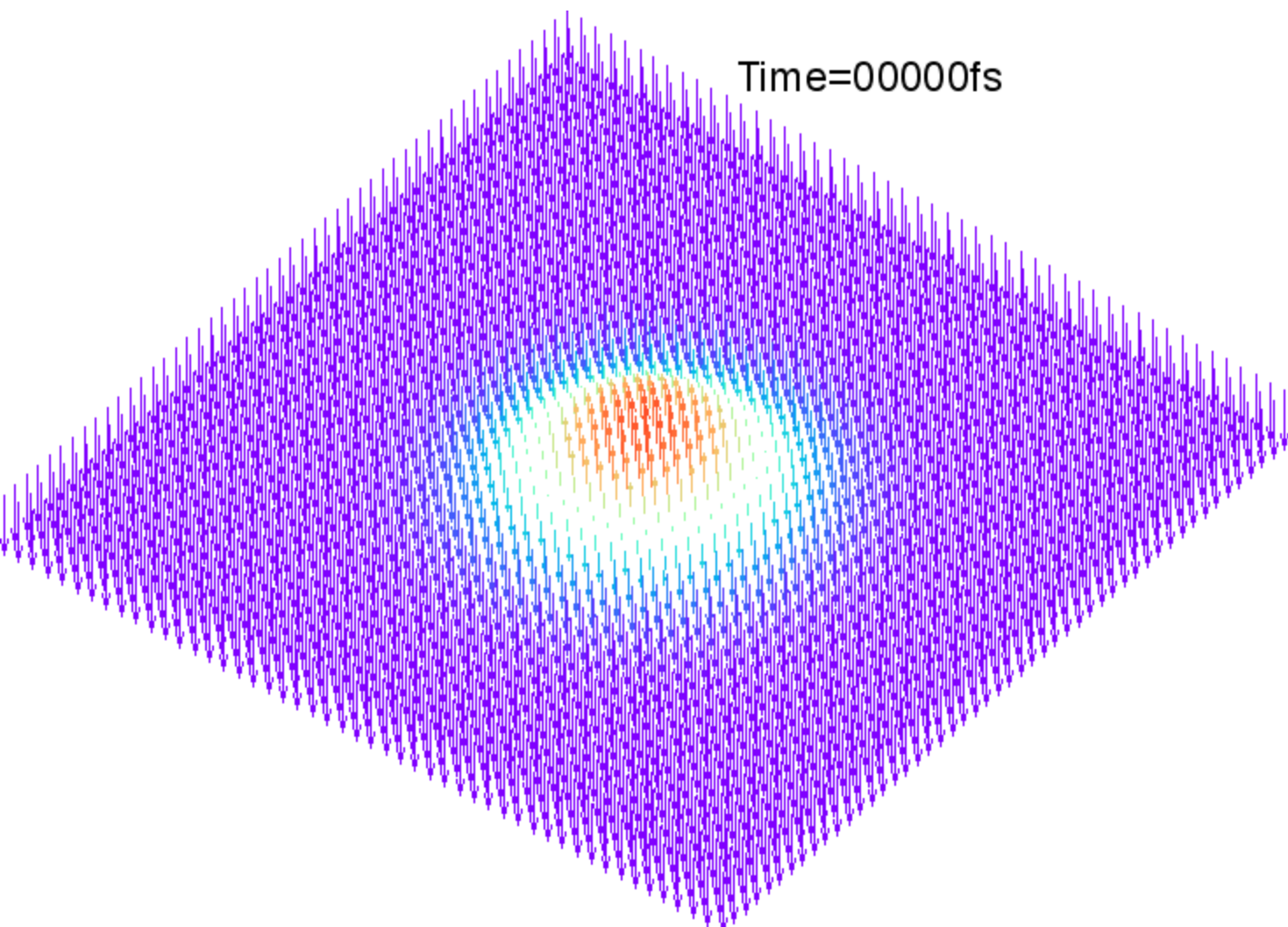
- [1] J. Stöhr and H. C. Siegmann, *Magnetism: From Fundamentals to Nanoscale Dynamics*, Springer-Verlag, Berlin, Heidelberg, New York (2006).
- [2] E. Beaurepaire, J. C. Merle, A. Daunois, and J.-Y. Bigot, Ultrafast spin dynamics in ferromagnetic nickel, *Phys. Rev. Lett.* **76**, 4250 (1996).
- [3] G. P. Zhang, W. Hübner, E. Beaurepaire, and J.-Y. Bigot, Laser-induced ultrafast demagnetization: Femtomagnetism, A new frontier? *Topics Appl. Phys.* **83**, 245 (2002).
- [4] A. Kirilyuk, A. V. Kimel, and Th. Rasing, Ultrafast optical manipulation of magnetic order, *Rev. Mod. Phys.* **82**, 2731 (2010). Erratum: *Rev. Mod. Phys.* **88**, 039904 (2016).
- [5] J. Walowski and M. Münzenberg, Perspective: Ultrafast magnetism and THz spintronics, *J. Appl. Phys.* **120**, 140901 (2016).
- [6] C. Boeglin, E. Beaurepaire, V. Halte, V. Lopez-Flores, C. Stamm, N. Pontius, H. A. Dürr, and J.-Y. Bigot, Distinguishing the ultrafast dynamics of spin and orbital moments in solids, *Nature* **465**, 458 (2010).
- [7] G. P. Zhang and W. Hübner, Laser-induced ultrafast demagnetization in ferromagnetic metal, *Phys. Rev. Lett.* **85**, 3025 (2000).
- [8] M. Wietstruk, A. Melnikov, C. Stamm, T. Kachel, N. Pontius, M. Sultan, C. Gahl, M. Weinelt, H. A. Dürr, and U. Bovensiepen, Hot-electron-driven enhancement of spin-lattice coupling in Gd and Tb 4*f* ferromagnets observed by femtosecond x-ray magnetic circular dichroism, *Phys. Rev. Lett.* **106**, 127401 (2011).
- [9] W. Töws and G. M. Pastor, Many-body theory of ultrafast demagnetization and angular momentum transfer in ferromagnetic transition metals, *Phys. Rev. Lett.* **115**, 217204 (2015).
- [10] V. Shokeen, M. Sanchez Piaia, J.-Y. Bigot, T. Müller, P. Elliott, J. K. Dewhurst, S. Sharma, and E. K. U. Gross, Spin flips versus spin transport in nonthermal electrons excited by ultrashort optical pulses in transition metals, *Phys. Rev. Lett.* **119**, 107203 (2017).
- [11] G. P. Zhang and M. Murakami, All-optical spin switching under different spin configurations, *J. Phys.: Condens. Matter* **31**, 345802 (2019).
- [12] E. Carpena, E. Mancini, C. Dallera, M. Brenna, E. Puppini, and S. De Silvestri, Dynamics of electron-magnon interaction and ultrafast demagnetization in thin iron films, *Phys. Rev. B*

- 78**, 174422 (2008).
- [13] M. Krauß, T. Roth, S. Alebrand, D. Steil, M. Cinchetti, M. Aeschlimann, and H. C. Schneider, Ultrafast demagnetization of ferromagnetic transition metals: The role of the Coulomb interaction, *Phys. Rev. B* **80**, 180407(R) (2009).
 - [14] C. Stamm, T. Kachel, N. Pontius, R. Mitzner, T. Quast, K. Holldack, S. Khan, C. Lupulescu, E. F. Aziz, M. Wietstruk, H. A. Dürr, and W. Eberhardt, Femtosecond modification of electron localization and transfer of angular momentum in nickel, *Nat. Mater.* **6**, 740 (2007).
 - [15] A. Baral, S. Vollmar, and H. C. Schneider, Magnetization dynamics and damping due to electron-phonon scattering in a ferrimagnetic exchange model, *Phys. Rev. B* **90**, 014427 (2014).
 - [16] C. Dornes *et al.*, The ultrafast Einstein-de Haas effect, *Nature* **565**, 209 (2019).
 - [17] B. Koopmans, G. Malinowski, F. Dalla Longa, D. Steiauf, M. Fähnle, T. Roth, M. Cinchetti, and M. Aeschlimann, Explaining the paradoxical diversity of ultrafast laser-induced demagnetization, *Nat. Mater.* **9**, 259 (2010).
 - [18] C. Illg, M. Haag, and M. Fähnle, Ultrafast demagnetization after laser irradiation in transition metals: Ab initio calculations of the spin-flip electron-phonon scattering with reduced exchange splitting, *Phys. Rev. B* **88**, 214404 (2013).
 - [19] M. Battiato, K. Carva, and P. M. Oppeneer, Superdiffusive spin transport as a mechanism of ultrafast demagnetization, *Phys. Rev. Lett.* **105**, 027203 (2010).
 - [20] A. Eschenlohr, M. Battiato, P. Maldonado, N. Pontius, T. Kachel, K. Holldack, R. Mitzner, A. Föhlisch, P. M. Oppeneer, and C. Stamm, Ultrafast spin transport as key to femtosecond demagnetization, *Nat. Mater.* **12**, 332 (2013).
 - [21] E. Turgut, C. La-o-vorakiat, J. M. Shaw, P. Grychtol, H. T. Nembach, D. Rudolf, R. Adam, M. Aeschlimann, C. M. Schneider, T. J. Silva, M. M. Murnane, H. C. Kapteyn, and S. Mathias, Controlling the competition between optically induced ultrafast spin-flip scattering and spin transport in magnetic multilayers, *Phys. Rev. Lett.* **110**, 197201 (2013).
 - [22] A. J. Schellekens, W. Verhoeven, T. N. Vader, and B. Koopmans, Investigating the contribution of superdiffusive transport to ultrafast demagnetization of ferromagnetic thin films, *Appl. Phys. Lett.* **102**, 252408 (2013).
 - [23] N. Moisan, G. Malinowski, J. Mauchain, M. Hehn, B. Vodungbo, J. Lüning, S. Mangin, E. E. Fullerton, and A. Thiaville, Investigating the role of superdiffusive currents in laser induced demagnetization of ferromagnets with nanoscale magnetic domains, *Sci. Rep.* **4**, 4658 (2014).

- [24] E. Turgut, D. Zusin, D. Legut, K. Carva, R. Knut, J. M. Shaw, C. Chen, Z. Tao, H. T. Nembach, T. J. Silva, S. Mathias, M. Aeschlimann, P. M. Oppeneer, H. C. Kapteyn, M. M. Murnane, and P. Grychtol, Stoner versus Heisenberg: Ultrafast exchange reduction and magnon generation during laser-induced demagnetization, *Phys. Rev. B* **94**, 220408 (2016).
- [25] G. P. Zhang, Y. H. Bai, T. Jenkins, and T. F. George, Laser-induced ultrafast transport and demagnetization at the earliest time: First-principles and real-time investigation, *J. Phys.: Condens. Matter* **30**, 465801 (2018).
- [26] B. Vodungbo *et al.*, Indirect excitation of ultrafast demagnetization, *Sci. Rep.* **6**, 18970 (2016).
- [27] M. van Kampen, C. Jozsa, J. T. Kohlhepp, P. LeClair, L. Lagae, W. J. M. de Jonge, and B. Koopmans, All-optical probe of coherent spin waves, *Phys. Rev. Lett.* **88**, 227201 (2002).
- [28] A. Melnikov, I. Radu, U. Bovensiepen, O. Krupin, K. Starke, E. Matthias, and M. Wolf, Coherent optical phonons and parametrically coupled magnons induced by femtosecond laser excitation of the Gd(0001) surface, *Phys. Rev. Lett.* **91**, 227403 (2003).
- [29] A. B. Schmidt, M. Pickel, M. Donath, P. Buczek, A. Ernst, V. P. Zhukov, P. M. Echenique, L. M. Sandratskii, E. V. Chulkov, and M. Weinelt, Ultrafast magnon generation in an Fe film on Cu(100), *Phys. Rev. Lett.* **105**, 197401 (2010).
- [30] M. Haag, C. Illg, and M. Fähnle, Role of electron-magnon scatterings in ultrafast demagnetization, *Phys. Rev. B* **90**, 014417 (2014).
- [31] R. Knut *et al.*, Inhomogeneous magnon scattering during ultrafast demagnetization, arXiv: 1810.10994v1 (2018).
- [32] I. Razdolski, A. Alekhin, N. Ilin, J. P. Meyburg, V. Roddatis, D. Diesing, U. Bovensiepen, and A. Melnikov, Nanoscale interface confinement of ultrafast spin transfer torque driving non-uniform spin dynamics, *Nat. Comm.* **8**, 15007 (2017).
- [33] S. Eich *et al.*, Band structure evolution during the ultrafast ferromagnetic-paramagnetic phase transition in cobalt, *Sci. Adv.* **3**, e1602094 (2017).
- [34] P. Tengdin, W. You, C. Chen, X. Shi, D. Zusin, Y. Zhang, C. Gentry, A. Blonsky, M. Keller, P. M. Oppeneer, H. C. Kapteyn, Z. Tao, and M. M. Murnane, Critical behavior within 20 fs drives the out-of-equilibrium laser-induced magnetic phase transition in nickel, *Sci. Adv.* **4**, eaap9744 (2018).
- [35] Z. H. Chen and L. W. Wang, private communication (2018).
- [36] E. Iacocca *et al.*, Spin-current-mediated rapid magnon localisation and coalescence after ul-

- trafast optical pumping of ferrimagnetic alloys, arXiv:1809.02076 (2018).
- [37] G. P. Zhang, Microscopic theory of ultrafast spin linear reversal, *J. Phys.: Condens. Mat.* **23**, 206005 (2011).
 - [38] G. P. Zhang, Y. H. Bai, and T. F. George, A new and simple model for magneto-optics uncovers an unexpected spin switching, *EPL* **112**, 27001 (2015).
 - [39] G. P. Zhang, Y. H. Bai, and T. F. George, Switching ferromagnetic spins by an ultrafast laser pulse: Emergence of giant optical spin-orbit torque, *EPL* **115**, 57003 (2016).
 - [40] G. P. Zhang, T. Latta, Z. Babyak, Y. H. Bai, and T. F. George, All-optical spin switching: A new frontier in femtomagnetism – A short review and a simple theory, *Mod. Phys. Lett. B* **30**, 1630005 (2016).
 - [41] G. P. Zhang, M. Murakami, M. S. Si, Y. H. Bai, and T. F. George, Understanding all-optical spin switching: Comparison between experiment and theory, *Mod. Phys. Lett. B* **32**, 1830003 (2018).
 - [42] B. Vodungbo, J. Gautier, G. Lambert, A. B. Sardinha, M. Lozano, S. Sebban, M. Ducouso, W. Boutu, K. Li, B. Tudu, M. Tortarolo, R. Hawaldar, R. Delaunay, V. Lopez-Flores, J. Arabski, C. Boeglin, H. Merdji, P. Zeitoun, and J. Lüning, Laser-induced ultrafast demagnetization in the presence of a nanoscale magnetic domain network, *Nat. Commun.* **3**, 999 (2012).
 - [43] J.-Y. Bigot and M. Vomir, Ultrafast magnetization dynamics of nanostructures, *Ann. Phys.* **525**, 2 (2013).
 - [44] M. S. Si and G. P. Zhang, Resolving photon-shortage mystery in femtosecond magnetism, *J. Phys.: Condens. Mat.* **22**, 076005 (2010).
 - [45] G. P. Zhang, Z. Babyak, Y. Xue, Y. H. Bai, and T. F. George, First-principles and model simulation of all-optical spin reversal, *Phys. Rev. B* **96**, 134407 (2017).
 - [46] S. Mathias, C. La-O-Vorakiat, P. Grychtol, P. Granitzka, E. Turgut, J. M. Shaw, R. Adam, H. T. Nembach, M. E. Siemens, S. Eich, C. M. Schneider, T. J. Silva, M. Aeschlimann, M. M. Murnane, and H. C. Kapteyn, Probing the timescale of the exchange interaction in a ferromagnetic alloy, *PNAS* **109**, 4792 (2012).
 - [47] G. P. Zhang, Y. Bai, W. Hübner, G. Lefkidis, and T. F. George, Understanding laser-induced ultrafast magnetization in ferromagnets: First-principles investigation, *J. Appl. Phys.* **103**, 07B113 (2008).
 - [48] K. Krieger, J. K. Dewhurst, P. Elliott, S. Sharma, and E. K. U. Gross, Laser-induced demag-

- netization at ultrashort time scales: Predictions of TDDFT, *J. Chem. Theory and Comput.* **11**, 4870 (2015).
- [49] K. Krieger, P. Elliott, T. Müller, N. Singh, J. K. Dewhurst, E. K. U. Gross, and S. Sharma, Ultrafast demagnetization in bulk versus thin films: An ab initio study, *J. Phys.: Condens. Mat.* **29**, 224001 (2017).
- [50] P. W. Granitzka *et al.*, Distinguishing local and non-local demagnetization in ferromagnetic FePt nanoparticles, arXiv:1903.08287 (2019).
- [51] B. Pfau *et al.*, Ultrafast optical demagnetization manipulates nanoscale spin structure in domain walls, *Nat. Commun.* **3**, 1100 (2012).
- [52] C. von Korff Schmising, B. Pfau, M. Schneider, C. M. Günther, M. Giovannella, J. Perron, B. Vodungbo, L. Müller, F. Capotondi, E. Pedersoli, N. Mahne, J. Lüning, and S. Eisebitt, Imaging ultrafast demagnetization dynamics after a spatially localized optical excitation, *Phys. Rev. Lett.* **112**, 217203 (2014).
- [53] V. Lopez-Flores, J. Arabski, C. Stamm, V. Halte, N. Pontius, E. Beaurepaire, and C. Boeglin, Time-resolved x-ray magnetic circular dichroism study of ultrafast demagnetization in a CoPd ferromagnetic film excited by circularly polarized laser pulse, *Phys. Rev. B* **86**, 014424 (2012).



Spin angular momentum